HHS Public Access

Author manuscript

Med Sci Sports Exerc. Author manuscript; available in PMC 2018 December 14.

Published in final edited form as:

Med Sci Sports Exerc. 2016 June ; 48(6): 990–1000. doi:10.1249/MSS.0000000000000884.

A Simple Hydraulic Analog Model of Oxidative Phosphorylation

Wayne T. Willis[1] **[Associate Professor]**, **Matthew R. Jackman**[2], **Jeffrey I. Messer**[3], **Sarah Kuzmiak-Glancy**[4], and **Brian Glancy**[5]

[1]Center for Metabolic and Vascular Biology, Arizona State University at Mayo Clinic, Scottsdale, AZ

[2]Division of Endocrinology, Department of Medicine, University of Colorado Anschutz Medical Campus, Aurora, CO

[3]Exercise Physiology Department, Mesa Community College, Mesa, AZ

[4]Department of Biomedical Engineering, The George Washington University, Washington, DC

[5]Laboratory of Cardiac Energetics, National Heart, Lung, and Blood Institute, National Institutes of Health, Bethesda, MD

Abstract

Mitochondrial oxidative phosphorylation is the primary source of cellular energy transduction in mammals. This energy conversion involves dozens of enzymatic reactions, energetic intermediates, and the dynamic interactions among them. With the goal of providing greater insight into the complex thermodynamics and kinetics ("thermokinetics") of mitochondrial energy transduction, a simple hydraulic analog model of oxidative phosphorylation is presented. In the hydraulic model water tanks represent the forward and back "pressures" exerted by thermodynamic driving forces: The matrix redox potential (ΔG_{redox}), the electrochemical potential for protons across the mitochondrial inner membrane (ΔG_{H^+}), and the free energy of ATP (ΔG_{ATP}). Net water flow proceeds from tanks with higher water pressure to tanks with lower pressure through "enzyme pipes" whose diameters represent the conductances (effective activities) of the proteins that catalyze the energy transfer. These enzyme pipes include the reactions of dehydrogenase enzymes, the electron transport chain (ETC), and the combined action of ATP synthase plus the ATP:ADP exchanger that spans the inner membrane. Additionally, reactive oxygen species production is included in the model as a leak that is driven out of the ETC pipe by high pressure (high ΔG_{redox}), and a proton leak dependent upon the ΔG_{H^+} for both its driving force and the conductance of the leak pathway. Model water pressures and flows are shown to simulate thermodynamic forces and metabolic fluxes that have been experimentally observed in mammalian skeletal muscle in response to acute exercise, chronic endurance training, and reduced substrate availability, as well as account for the thermokinetic behavior of mitochondria from fast- and slow-twitch skeletal muscle and the metabolic capacitance of the creatine kinase reaction.

Corresponding Author: Wayne T. Willis, Associate Professor, Center for Metabolic and Vascular Biology, ASU at Mayo Clinic, Mail Code 3020, 13208 E. Shea Blvd., Mayo Clinic CRB 2-228, Scottsdale, AZ 85259, (480)301-9198, Fax, (480)301-7017, waynewillis@asu.edu.

Keywords

mitochondria; energy transduction; Gibbs free energy; non-equilibrium thermodynamics

Mitochondrial Energy Transduction

Mitochondria combust fuels to CO_2 and H_2O and convert the energy released to ATP free energy (ΔG_{ATP}). As shown schematically in Figure 1A, the energy transduction takes place in three major steps: 1) Dehydrogenase (DH) enzymes collect electrons from fuels, which generates a matrix oxidation-reduction potential (ΔG_{redox}) down the electron transport chain (ETC). 2) The ETC converts ΔG_{redox} energy into an electrochemical potential for protons (ΔG_{H^+}) across the inner mitochondrial membrane. This transduction is achieved by coupling electron flow down the voltage drop of the ETC to the translocation ("pumping") of protons across the inner membrane (from the matrix toward the cytosol). The proton electrochemical gradient (ΔG_{H^+}) so generated is the sum of electrical ($\Delta\Psi$) and chemical (ΔpH) potentials and is sometimes referred to as the "protonmotive force" (Δp). 3) Finally, F_1-ATP synthase (Complex V) uses proton flux from cytosol to matrix driven by ΔG_{H^+} to phosphorylate ADP in the mitochondrial matrix. Matrix ATP^{4-} is then translocated to the cytosol in exchange for cytosolic ADP^{3-} by the adenine nucleotide translocase (ANT), which is driven by the $\Delta\Psi$ component of ΔG_{H^+}. Along the way, two energy dissipation processes can occur: 1) Single electron (monovalent) reduction of an O_2 molecule to the superoxide radical ($O_2^{\cdot -}$) is a free radical initiation reaction sometimes called the "electron leak" and 2) ΔG_{H^+} can drive H^+ across the inner membrane back into the matrix via pathways other than Complex V. Under physiological conditions, the electron leak rate represents a very small, <0.1%, fraction of the electrons transported down the ETC. In contrast, the proton leak rate can, under certain conditions, dissipate a substantial fraction of the energy released from fuel oxidation (7).

Mitochondrial Energy Transduction is a Linear Force:Flow Relationship

Recently, Robert Balaban's laboratory (16) showed in mitochondria isolated from pig skeletal muscle that each of the three major steps of oxidative phosphorylation in Figure 1 can be described with a linear force:flow relationship:

$$\text{Flow} = (\text{Net Driving Force}) \times (\text{Conductance}) \quad [1]$$

Ohm's Law is perhaps the most familiar example of such a linear force:flow relationship, in which flow is current, net driving force is voltage, and conductance is the reciprocal of resistance. In mitochondrial oxidative phosphorylation flow is metabolic flux (which takes various forms in the pathway, see below), net driving force is the difference between two free energies ($\Delta\Delta G$), and conductance is the reciprocal of enzyme/enzyme pathway resistance to metabolic flow.

Energy and Stoichiometry of Each Step

In order to calculate the net driving force (ΔΔG) of a step, for example ($\Delta G_{redox} - \Delta G_{H^+}$), each energy must be adjusted by the appropriate stoichiometry and in some cases a conversion factor such as the Faraday to match the units. For example, down the entire ETC this stoichiometry is 10 protons translocated ("pumped") for each pair of electrons that reduce ½O_2 to H_2O (49), a stoichiometry of ($10H^+$):($2e^-$). Thus, each pair of electrons traveling down the ETC encounters the "backpressure" of 10 protons, which opposes net electron advancement. The net driving force through the step is the difference: ($2e^-$x ΔG_{redox}) minus ($10H^+$ x ΔG_{H^+}). Similarly, the stoichiometry of ΔG_{H^+} to ΔG_{ATP} conversion must take into account the protons used for both the matrix synthesis of ATP and the inner membrane exchange of ATP-for-ADP and transport of inorganic phosphate. These stoichiometries are $2\frac{2}{3}$ H^+ per matrix ATP synthesized ($8H^+$/3ATP) at Complex V (68), plus the ΔG_{H^+} of one additional H^+ to power ADP^{3-}:ATP^{4-} exchange at ANT ($\Delta\Psi$ component of ΔG_{H^+}) (8) and inorganic phosphate (Pi) transport into the matrix via the phosphate transporter (ΔpH component of ΔG_{H^+}), for a total of $3\frac{2}{3}$ H^+ per cytosolic ATP. Again, the net driving force through the step is the difference: ($3\frac{2}{3}$ x ΔG_{H^+}) minus (ΔG_{ATP}). In this review, we seek the clarity offered by the simplicity of Equation 1, and so we will not proceed to the quantitative relationships used to calculate oxidation-reduction potential difference down the ETC and its conversion to redox free energy (ΔG_{redox}), the electrochemical potential for protons across the inner membrane (ΔG_{H^+}), and the chemical free energy of cytosolic ATP (ΔG_{ATP}). Instead, the reader is referred to the lucid presentation of these ideas by Nicholls and Ferguson (49), who over 30 years ago began making these difficult concepts accessible to the rest of us in their Bioenergetics series (49). In addition, Glancy et al. describe in quantitative terms how the apparent conductance of each step is determined from the experimental measurements of flow and these net driving forces (16).

Hydraulic Model

Linear force:flow relationships along at least some portion of the oxidative pathway were experimentally demonstrated by numerous visionary pioneers in the field of mitochondrial bioenergetics, such as Rottenberg (57), Klingenberg (52), Van Dam (66), Westerhoff (69), Stucki (62), Wanders (67), Davis (12), Lemasters (39), Brand (48), Nicholls (50), Balaban (31), Wilson (72) and others. All were inspired by Onsager's Nobel-winning contributions (53, 54). We have developed a simple hydraulic analog model to make Mitchell's chemiosmotic theory (46) more approachable for specialists and non-specialists alike. This hydraulic model is shown in Figure 1B. The three energetic intermediates ("pools") mentioned above, ΔG_{redox}, ΔG_{H^+}, and ΔG_{ATP}, are represented by water tanks. The water level (pressure) of each tank corresponds to the free energy and stoichiometry of that intermediate. Equal water levels correspond to thermodynamic equilibrium between two intermediates. Net water flow obviously proceeds from higher pressure to lower pressure. The energy tanks are connected by enzyme pipes. The diameter of each pipe represents the conductance (inverse of resistance) of that step; large diameter pipes represent high abundance (or high V_{max}) enzymes, while narrow pipes indicate high resistance to flow (low

abundance or V_{max}). Flow between any two tanks is therefore given by Equation 2, Poiseuille's Law, which, of course, takes the same form as Equation 1:

$$\text{Water flow} = (\text{pressure difference}) \times (\text{pipe conductance}) \quad [2]$$

Under laminar water flow conditions, pipe conductance can be calculated as: $\Pi\ r^4/(8\ \eta\ L)$, where r is pipe radius, η is water viscosity, and L is pipe length. Because physical flow, energetic driving force, and conductance are arranged identically in both the analog model and the energy transductions of the target system they describe, this hydraulic model could be described as a "formal analogy" of oxidative phosphorylation. Water outflow through an "ATPase" pipe (cytosolic ATP breakdown) drives energy-requiring (endergonic) processes, such as muscle contraction, ion pumping, or biosynthesis (the water outflow could be shown turning a paddle wheel, for example). In Figure 1B, which depicts a "resting skeletal muscle cell," the ATPase valve is barely open, with just enough water (ATP) flow to power the basic "housekeeping" functions of resting tissue. As a result, very little pressure drop is required from $\Delta G_{redox} \rightarrow \Delta G_{H^+} \rightarrow \Delta G_{ATP}$. The height of the ΔG_{redox} tank is set by water flow delivered from a Fuel tank through a dehydrogenase (DH) pipe. This flow is driven by a "substrate pressure" (water height in the fuel tank), which is the extent of DH enzyme saturation: Fractional saturation = $[S]/([S] + K_M)$. Fuel inflow to the ΔG_{redox} tank is resisted by the diameter of the DH pipe and also by a float valve representing kinetic feedback inhibition by products of the substrate oxidation (e.g., high $NADH/NAD^+$ and Acetyl CoA/CoA ratios). It should be noted that, while the model shows only one DH pipe, in reality there are many "dehydrogenase input pipes" in mitochondria. Further, only those DH steps that are NAD-linked, for example pyruvate dehydrogenase and beta-hydroxyacyl CoA dehydrogenase, deliver electrons to NADH and Complex I of the ETC as shown in the model. In other words, this model can be expanded upon to include multiple fuel inflow pipes if mitochondrial fuel selection is the discussion of interest.

Leak Reactions

Superoxide production (e^- leak) is depicted as water leaving the top of a pipe that represents the ETC pathways by which single electrons leave an ETC carrier and monovalently reduce molecular O_2 to the superoxide radical, $O_2^{\cdot -}$. As shown in this resting condition with high fuel availability, the "pressures" (water heights) of the ΔG_{redox} and ΔG_{H^+} tanks are robust and above the top of the e^- leak pipe (Fig. 1B). Thus, "high pressure ETC water" (highly reduced ETC electron carriers) is shown leaking from the top of the e^- leak pipe, simulating the production of superoxide radicals. Similarly, the proton leak pathway is shown as a leak pipe projecting from the ΔG_{H^+} tank, because proton backleak across the inner membrane is driven by ΔG_{H^+}, according to: $J_{H^+leak} = \Delta G_{H^+} \times C_{M,H^+}$ (where C_{M,H^+} is the apparent conductance of this leak pathway). There is the potential for much greater leak flow through this higher conductance proton leak pathway. Brand and coworkers have clearly shown that, at least in mitochondria isolated from skeletal muscle and liver, proton leak kinetics are "non-Ohmic," meaning that the apparent conductance (C_{M,H^+}) is not a constant value, but rather rises with the driving force, ΔG_{H^+} (4). Our own data from experiments on rat liver mitochondria (unpublished observations by Dr. Carrie Lyons) shown in Figure 2, illustrate

this non-Ohmic behavior. Non-Ohmic kinetics are simulated in the model with a float valve that opens the proton leak pipe as the ΔG_H^+ "water level" rises. Thus, both the driving force (water height above the leak pipe), as well as the pipe conductance, increase as ΔG_H^+ rises. Note that a larger diameter proton leak pipe would tend to lower both ΔG_{redox} and ΔG_H^+, thus reducing superoxide flow from the e^- pipe. This feature of the model simulates the protective antioxidant effect that proton leak might offer, as conceptualized by both Brand and Skulachev in their "uncoupling to survive" hypothesis (6, 60).

Both electron leak and proton leak contribute to the complexity of the mitochondrial energy transduction pathway. The representations of these two leak pathways within the hydraulic model provide a simple analogy to explain these intricacies. For example, while students often find it intuitive that an increase in proton leak dissipates ΔG_H^+ and decreases ATP synthesis, they may struggle to understand why this is associated with an increase in O_2 consumption rate. Using the hydraulic model as a simulator, it is obvious that increasing the diameter of the proton leak pipe would naturally increase water flow through the ETC pipe (increase O_2 consumption rate), while water flow through the C V + ANT pipe (ATP production rate) could remain very low or zero.

Transition to Exercise

In transition to the contractile activity of mild exercise, a Ca^{2+} signal opens the ATPase valve sufficiently for water outflow through the ATPase to match the increased energy demand (Figure 3A). The moment the ATPase valve opens, a metabolic transient ensues in which water outflow through the ATPase exceeds water delivery coming from the CV + ANT pipe (70). The ΔG_{ATP} tank water level therefore begins to fall, creating a greater pressure drop from $\Delta G_H^+ \rightarrow \Delta G_{ATP}$. This greater pressure head elicits greater water flow through CV + ANT and, in turn, the ΔG_H^+ water height falls and so on upstream, until all flows are again equal in every segment and equal to the outflow through the ATPase. The result is a new, steady state, higher flow rate with lower water levels in every tank (except, usually, the fuel reservoir, which has immense capacitance relative to the other tanks; see below for elaboration of this capacitance issue). In comparing Figure 3A to Figure 1B, note that in transition from "resting" to "mild exercise" the energy level of the ΔG_{ATP} tank went from about "9 energy units" down to about 7½, while ΔG_H^+ fell from about 9½ to about 8½, etc.

The Leaks "Dry Up" in Transition to Exercise

As shown in Figure 3B, transition to a higher, moderate exercise intensity demands yet higher flow through the system, resulting in even lower steady state water tank heights. Under these conditions, the reduced pressures "upstream" withdraw the driving forces for the leaks. As a consequence, transition to higher ATP demand has a "drying up" effect on both the proton and electron (32, 61) leaks.

Increasing Pipe Diameters: Ca^{2+} and Greater Abundance (endurance training)

Table 1 summarizes the apparent resistance of each mitochondrial segment in pig mixed skeletal muscle mitochondria, as determined by Glancy et al. (16). In each case, resistances are expressed in the electrical units of Ohms, which were calculated as described above using the appropriate stoichiometries and conversion constants. Two patterns are obvious: 1) The ETC is the segment with the most resistance to energy transfer and 2) Ca^{2+} acutely reduces the resistance of every segment by a factor of about two. In the hydraulic analog model, therefore, the "ETC pipe" should have the smallest diameter and Ca^{2+} should acutely make all pipes grow wider. Thus, what was not depicted in the transition from Figure 1B to either Figure 3A or B were increased pipe diameters that would attend the Ca^{2+} activation of the ATPase. The concomitant Ca^{2+} widening (activation) of the mitochondrial "pipes" would reduce the magnitude of the energy drops required to elicit the higher flux during exercise. However, it is important to emphasize that in skeletal muscle this compensatory influence of Ca^{2+} merely ameliorates the fall in energy status that occurs in the transition from rest to exercise; rising cytosolic [Ca^{2+}] does not eliminate the requirement for an energy decline when ATP demand rises. Stated yet another way, in skeletal muscle a fall in cytosolic ΔG_{ATP} is always observed in transition from a lower to a higher energy turnover rate (10). In cardiac muscle, in contrast, Ca^{2+} activation of the mitochondrial pathway is extreme, proportionally matching the Ca^{2+} activation of ATPases. Balaban has shown in cardiac muscle *in vivo* that this Ca^{2+}-mediated "parallel activation" mechanism obviates any fall in energy levels when hearts transition from one ATP turnover to a higher one (2).

Endurance Training

John Holloszy's landmark study of 1967 revealed that endurance training increases the mitochondrial content of skeletal muscle (22). Trained muscle is therefore modeled with larger pipes, as shown in Figure 3C. Compared to Figure 3B, the "bigger pipes" of trained muscle allow the same flow (same exercise intensity) to be achieved with smaller pressure gradients. The model simulates the improved defense of energetic homeostasis observed after a program of endurance training, as experimentally demonstrated by Dudley, Tullson, and Terjung in 1987 (13). Similar to many *in vitro* experiments performed by Phil Gollnick (personal communication), our data shown in Figure 3D demonstrate this concept. Viewed one way, doubling the mitochondrial content in the system doubles the oxidative flux at a given ATP free energy (thus doubling mitochondrial power output, see below). Another view is that a given flux (a given exercise intensity) is achieved at a more negative (more robust) ATP free energy in the "trained" system (see horizontal line corresponding to 40 nmol O_2/min). Decades ago, Holloszy described (24) this concept that training-induced increases in muscle mitochondrial content enable better defense of energy phosphate status in response to a given intensity of exercise (in the model, higher water levels at a given flow). The important consequences of this stronger homeostatic defense on fuel selection have been elucidated by many of Holloszy's postdoctoral trainees [e.g., Bob Fitts (14), Frank Booth (23), Ron Terjung (64), and Ken Baldwin (3)]. Connett (9, 11) and Saltin and Gollnick (18)

also offered insightful metabolic models that predicted the carbohydrate-sparing effect mediated by the elevated mitochondrial content of endurance-trained skeletal muscle.

Substrate Availability

In Figure 4, the same trained muscle exercising at the same intensity as in Figure 3C now encounters declining fuel availability (fuel tank water level has fallen from nearly 1.0 to 0.6). For simplicity, let's consider this perturbation as an instantaneous step change. The decreased fuel pressure would initiate a transient in which water delivery through the "DH pipe" would suddenly fail to match the flows below. The imbalance would first cause a fall in $\Delta G_{redox,}$ which would have a series of consequences: 1) Downstream, the ($\Delta G_{redox} - \Delta G_{H^+}$) pressure head, thus flow through the ETC pipe, would decrease lowering the ΔG_{H^+} level. This pattern would continue to propagate downstream into the (Complex V + ANT) pipe and ΔG_{ATP} tank. 2) Upstream, however, the falling float valve in the ΔG_{redox} tank (less NADH feedback inhibition) would restore flow through the DH pipe and, similarly, the falling water levels in the ΔG_{H^+} and ΔG_{ATP} tanks would also elicit "recoil" recoveries in the pipe flows upstream of them. Once steady state conditions were fully restored (flows equal in all pipes), one clear outcome of this fuel perturbation would be lower water levels (energetic driving forces) in every tank. But, an intriguing question is whether the system would recover to the original flow at these lower energy levels? This simple example reveals that the hydraulic model forces us to consider the connectivity property of metabolic control analysis (21, 28). If flow out of the ATPase pipe is insensitive to the ΔG_{ATP} tank water level, then flow should recover to the initial, pre-fuel depleted, rate. However, if it is sensitive i.e, if the ATPase *has finite negative elasticity to the energy available from ATP*, then fuel depletion would require additional stimulation of the ATPase (more Ca^{2+} signal to open the ATPase pipe further) to fully recover the initial flow rate. This is, in fact, observed during prolonged exercise. As Gollnick and Saltin demonstrated, the progressive depletion of muscle glycogen elicits greater and greater recruitment of higher threshold motor units (17). In the context of the illuminating studies by Jeneson et al. (26), this may reflect a redistribution of flux control away from the module of ATP utilization, the ATPase (and, indeed, away from the central nervous system), and toward the module of ATP production, mitochondria. Consistent with these ideas, carbohydrate depletion during prolonged moderate-to-heavy intensity exercise to exhaustion results in an unchanging flux (VO_2), progressively falling muscle [PCr] (ΔG_{ATP}), greater motor unit activation, and a rising perception of effort (65). In this fuel-depletion scenario, the model simulates the *in vivo* data of Sahlin's laboratory (58) and our *in vitro* results. Messer et al. (42) showed that as sub-saturating concentrations of either malate or pyruvate were decreased i.e., as the ratio $[S]/([S]+K_M)$ fell, a given flux required a lower (less negative or less robust) ΔG_{ATP}.

ATP: Biological "Energy Currency"

Both the training scenario, which enhanced mitochondrial defense of ATP free energy, and substrate depletion, which degraded it, address the critical issue of ΔG_{ATP} homeostasis. The hydraulic model provides intuitive appreciation that mitochondria perform two equally important functions related to cellular energy metabolism: 1) ATP synthesis (J_p) and 2) defense of ΔG_{ATP}. The product of these two variables is the power output of mitochondria

(mP_o): $mP_o = J_p \times \Delta G_{ATP}$, which drives ATP-utilizing processes. In other words, the analogy of ATP as biological "energy currency" should include both features of a currency, units of exchange ("bills" = ATP molecules) and denominations ("bill value" = free energy of ATP i.e., ΔG_{ATP}). Just as devalued currency has less purchasing power, mitochondria in untrained or fuel-depleted muscle generate ATP that delivers a diminished driving force to an endergonic process such as force production or ion pumping. This simple hydraulic model clearly demonstrates that, while falling ΔG_{ATP} stimulates metabolic flow from upstream driving forces, increasing the ATP synthesis rate, it also diminishes the "pressure" of each ATP delivered to sites of ATP utilization. Indeed, Roger Cooke has shown that actomyosin force production declines linearly as log[Pi] rises (hence ATP hydrolysis delivers less driving force) (55). Masuda, Dobson, and Veech showed similar linear dependence of ΔG_{ATP} with the Na^+ gradient maintained across the sarcolemma of rodent ventricles (41), and Hasselbach demonstrated that the cytosolic-sarcoplasmic reticulum Ca^{2+} gradient is also proportional to ΔG_{ATP} (20). A skeletal muscle mitochondrial system "weakened" by a lack of training or fuel scarcity must allow greater devaluation of ATP currency to match a given demand. But, because the ATP stoichiometry of cellular ATPases is fixed, to the extent ΔG_{ATP} falls, force production by actomyosin (56) and ion gradients across sarcolemmal (41) and sarcoplasmic reticulum (29) membranes also may deteriorate.

Mitochondria in Type I and Type II Muscle Fibers

Compared to type II (white, fast, glycolytic) fibers, type I (red, slow, oxidative) muscle cells typically contain 2–3 times more mitochondrial protein (59) and as little as ½ the total creatine (PCr + Cr) (35). Curiously, at rest, feline type II biceps muscle fibers maintain a much more robust (more negative) ATP free energy than type I soleus, despite essentially identical mass-specific VO_2 (33). As seen in Figure 5A, mitochondria isolated in our lab by Matt Jackman behaved similarly: higher (more negative) "static head" ΔG_{ATP} was developed by rabbit gracilis (99% type IIb) compared to soleus (98% type I). Previously Jackman and Willis reported 2-fold higher NAD-linked isocitrate dehydrogenase (IDH) and glycerol-3-phosphate (G3P) dehydrogenase activities in these type IIb compared to type I mitochondria (25). IDH is generally considered a critical locus of flux control in the citric acid cycle and G3P oxidation is a well-known source of superoxide production (47). In the hydraulic model, type IIb mitochondria would therefore, in relative terms, have a larger DH pipe diameter, which is consistent with the ability to develop higher static head ΔG_{redox}, and thus, ΔG_{ATP} (Figure 5A). This, coupled with lower conductance downstream (see the diminished slope in Figure 5A), suggests greater tendency to fuel the electron leak, even as downstream pressures are "relaxed" by transition to higher flow. This prediction is experimentally supported by Figures 5B and C. Notice that white muscle mitochondria generate much higher superoxide ("e^- leak") with the glycolytic substrates shown (and particularly with the substrates of the cytosolic-mitochondrial electron shuttles). The concept of cost-benefit tradeoff therefore emerges from the hydraulic model. Because the creatine kinase reaction is maintained near to equilibrium, higher static head ΔG_{ATP}, thus a higher cytosolic ATP/ADP ratio, means a high PCr/Cr ratio, which is an obvious benefit to a fiber tailored for rapid transition to high power output. But the cost may be that the high "upstream pressures" required to develop this higher "ATP pressure" predict the potential for higher free radical

production, which is consistent with Brian Glancy's data from our lab shown in Figures 5B and C.

PCr and Creatine Kinase: Metabolic Capacitance

Figure 6A expands the model to include the concept of metabolic capacitance (63). A high volume phosphocreatine (PCr) tank is added and linked to the ATP tank by two large diameter creatine kinase pipes, CK_m (CK located in the mitochondrial intermembrane space) and CK_c (cytosolic CK). The high volume of this tank simulates both high PCr concentration and the large equilibrium constant of the CK reaction. The large diameter of these CK pipes reflects the extremely high catalytic potential (V_{max}) of cellular creatine kinase, which has been shown to maintain near-thermodynamic equilibrium between cytosolic ΔG_{ATP} and ΔG_{PCr} across essentially the entire range of aerobic ATP turnover (34). As shown in Figure 6B, in transition to contractile activity the opening of the ATPase valve will, as before, cause the ΔG_{ATP} water level to fall. But the capacitance of the high volume PCr tank dramatically reduces the rate at which the ATP water level declines. Nevertheless, as always, an aerobic steady state can only be achieved when the flow at the ATPase (ATP demand) is matched by delivery from the fuel tank, and each step therefore must attain the same pressure difference according to Equation 2. Therefore, *with or without the PCr tank*, the pressure difference required for steady state is:

$$\text{pressure drop} = \text{flow/conductance} \quad [3]$$

The presence of the PCr tank and CK pipes changes neither the steady state flow nor the conductances of the other pipes, so the magnitude of the pressure drops from $\Delta G_{redox} \rightarrow \Delta G_{H^+} \rightarrow \Delta G_{ATP}$ required to achieve steady state remain unchanged. The addition of PCr simply extends the time required to achieve those lower steady state water levels. In Figures 6B and 6C, the hydraulic model depicts the delayed "kinetics of O_2 uptake" observed in the presence of CK and PCr (15, 44). Notice that, at all times, the water levels of the PCr and ATP tanks remain nearly equal; near equilibrium between the PCr and ATP pools is ensured by the high CK V_{max} (large diameter pipe). As clearly described by Ron Meyer, H. Lee Sweeney, and Martin Kushmerick, the "additional water" of the PCr tank simply offers metabolic capacitance to the system and therefore extends the time required to achieve steady state (19, 27, 30, 43, 45).

The "Creatine Kinase Energy Clamp"

With the generous guidance of Richard Connett, we adapted these ideas to develop a methodological tool with which to study mitochondrial metabolism at constant, experimentally-established ATP free energy levels, the "Creatine Kinase Energy Clamp" (Figure 6D). This procedure takes advantage of the immense capacitance that mM levels of PCr+Cr in a buffering medium impose upon microgram quantities of respiring mitochondria. In the CK clamp, 5 mM ATP, 5–30 mM TCr (total creatine = PCr+Cr), and saturating activity of CK are added to ensure complete equilibrium is maintained between ATP/ADP and PCr/Cr. Figure 6D shows that CK simply acts as the ATPase in the procedure, and the

essentially infinite capacitance of the total creatine pool ensures that a constant and experimentally set ΔG_{ATP} "backpressure" opposes mitochondrial flux (measured as O_2 consumption rate). As developed in Messer et al. (42), this clamp has complete concentration control of the ATP turnover loop, leaving mitochondria, therefore, with complete flux control (5). This procedure was utilized in the experiments depicted in Table 1 and Figures 3D and 5 and has also been used to investigate fuel selection, insulin resistance, oxygen uptake kinetics, and Ca^{2+} activation of skeletal muscle mitochondria from rats, pigs, sparrows, and/or humans (15, 16, 36–38, 42).

Conclusions

Our aim in developing the hydraulic analog model was to provide a simple analogy with which to view the complex thermodynamics and kinetics that underlie the control of mitochondrial oxidative phosphorylation. An added benefit of using a hydraulic analog system is the laws governing water flow are structurally similar to the non-equilibrium thermodynamic relationships that can describe the major steps of oxidative phosphorylation. As a result, the model can closely simulate the thermodynamic forces and metabolic flows that are routinely observed in different muscle cell types in response to a variety of environmental perturbations. The hydraulic analog model is a simple and effective teaching tool, and might also provide a framework to plan and interpret studies of mitochondrial bioenergetics.

Acknowledgements

The authors would like to thank Jeremy Oxley and Leonard Eidson for constructing the first physical prototype of the hydraulic model almost 15 years ago. This work was supported by a grant from the National Science Foundation (IBN-0116997). The authors declare no conflicts of interest. The results of the present study do not constitute endorsement by ACSM.

References

1. Ackrell BA, Maguire JJ, Dallman PR, Kearney EB. Effect of iron deficiency on succinate-and NADH-ubiquinone oxidoreductases in skeletal muscle mitochondria. J Biol Chem 1984;259(16): 10053–9. [PubMed: 6432778]
2. Balaban RS, Kantor HL, Katz LA, Briggs RW. Relation between work and phosphate metabolite in the in vivo paced mammalian heart. Science 1986;232(4754):1121–3. [PubMed: 3704638]
3. Baldwin KM, Fitts RH, Booth FW, Winder WW, Holloszy JO. Depletion of muscle and liver glycogen during exercise. Protective effect of training. Pflugers Arch 1975;354(3):203–12. [PubMed: 1167678]
4. Brand MD. The proton leak across the mitochondrial inner membrane. Biochim Biophys Acta 1990;1018(2–3):128–33. [PubMed: 2393654]
5. Brand MD. Top down metabolic control analysis. J Theor Biol 1996;182(3):351–60. [PubMed: 8944168]
6. Brand MD. Uncoupling to survive? The role of mitochondrial inefficiency in ageing. Exp Gerontol 2000;35(6–7):811–20. [PubMed: 11053672]
7. Brand MD, Chien LF, Ainscow EK, Rolfe DF, Porter RK. The causes and functions of mitochondrial proton leak. Biochim Biophys Acta 1994;1187(2):132–9. [PubMed: 8075107]
8. Bremer J, Davis EJ. Studies on the active transfer of reducing equivalents into mitochondria via the malate-aspartate shuttle. Biochim Biophys Acta 1975;376(3):387–97. [PubMed: 164904]

9. Connett R Analysis of metabolic control: new insights using a scaled creatine kinase model. Am J Physiol 1988;254:R949–R59. [PubMed: 2837918]
10. Connett R, Honig C. Regulation of VO2 in red muscle: do current biochemical hypotheses fit in vivo data. Am J Physiol 1989;256(25):R898–R906. [PubMed: 2705578]
11. Connett RJ. In vivo control of phosphofructokinase: system models suggest new experimental protocols. Am J Physiol 1989;257(4 Pt 2):R878–88. [PubMed: 2529783]
12. Davis E, Davis-Van Thienen W. Force-flow and back-pressure relationships in mitochondrial energy transduction: an examination of extended state 3-state 4 transitions. Arch Biochem Biophys 1989;275:449–58. [PubMed: 2596850]
13. Dudley G, Tullson P, Terjung R. Influence of mitochondrial content on the sensitivity of respiratory control. J Biol Chem 1987;262:9104–14.
14. Fitts RH, Booth FW, Winder WW, Holloszy JO. Skeletal muscle respiratory capacity, endurance, and glycogen utilization. Am J Physiol 1975;228(4):1029–33. [PubMed: 165725]
15. Glancy B, Barstow T, Willis WT. Linear relation between time constant of oxygen uptake kinetics, total creatine, and mitochondrial content in vitro. Am J Physiol Cell Physiol 2008;294(1):C79–87. [PubMed: 17942641]
16. Glancy B, Willis WT, Chess DJ, Balaban RS. Effect of calcium on the oxidative phosphorylation cascade in skeletal muscle mitochondria. Biochemistry 2013;52(16):2793–809. [PubMed: 23547908]
17. Gollnick PD, Armstrong RB, Saubert CWt, Sembrowich WL, Shepherd RE, Saltin B Glycogen depletion patterns in human skeletal muscle fibers during prolonged work. Pflugers Arch 1973;344(1):1–12. [PubMed: 4272644]
18. Gollnick PD, Saltin B. Significance of skeletal muscle oxidative enzyme enhancement with endurance training. Clin Physiol 1982;2(1):1–12. [PubMed: 7201906]
19. Grassi B, Rossiter HB, Hogan MC, et al. Faster O(2) uptake kinetics in canine skeletal muscle in situ after acute creatine kinase inhibition. J Physiol 2011;589(Pt 1):221–33. [PubMed: 21059760]
20. Hasselbach W, Oetliker H. Energetics and electrogenicity of the sarcoplasmic reticulum calcium pump. Annu Rev Physiol 1983;45:325–39. [PubMed: 6303204]
21. Heinrich R, Rapoport TA. A linear steady-state treatment of enzymatic chains. General properties, control and effector strength. Eur J Biochem 1974;42(1):89–95. [PubMed: 4830198]
22. Holloszy JO. Biochemical adaptations in muscle. Effects of exercise on mitochondrial oxygen uptake and respiratory enzyme activity in skeletal muscle. J Biol Chem 1967;242(9):2278–82. [PubMed: 4290225]
23. Holloszy JO, Booth FW. Biochemical adaptations to endurance exercise in muscle. Annu Rev Physiol 1976;38:273–91. [PubMed: 130825]
24. Holloszy JO, Coyle EF. Adaptations of skeletal muscle to endurance exercise and their metabolic consequences. J Appl Physiol 1984;56(4):831–8. [PubMed: 6373687]
25. Jackman MR, Willis WT. Characteristics of mitochondria isolated from type I and type IIb skeletal muscle. Am J Physiol 1996;270(2 Pt 1):C673–8. [PubMed: 8779934]
26. Jeneson JA, Westerhoff HV, Kushmerick MJ. A metabolic control analysis of kinetic controls in ATP free energy metabolism in contracting skeletal muscle. Am J Physiol Cell Physiol 2000;279(3):C813–32. [PubMed: 10942732]
27. Jones AM, Wilkerson ΔΠ, Fulford J. Influence of dietary creatine supplementation on muscle phosphocreatine kinetics during knee-extensor exercise in humans. American Journal of Physiology-Regulatory Integrative and Comparative Physiology 2009;296(4):R1078–R87.
28. Kacser H, Burns JA. The control of flux. Biochem Soc Trans 1995;23(2):341–66. [PubMed: 7672373]
29. Kammermeier H, Schmidt P, Jungling E. Free energy change of ATP-hydrolysis: a causal factor of early hypoxic failure of the myocardium? J Mol Cell Cardiol 1982;14(5):267–77. [PubMed: 7131563]
30. Kindig CA, Howlett RA, Stary CM, Walsh B, Hogan MC. Effects of acute creatine kinase inhibition on metabolism and tension development in isolated single myocytes. J Appl Physiol 2005;98(2):541–9. [PubMed: 15333609]

31. Koretsky AP, Balaban RS. Changes in pyridine nucleotide levels alter oxygen consumption and extra-mitochondrial phosphates in isolated mitochondria: a 31P-NMR and NAD(P)H fluorescence study. Biochim Biophys Acta 1987;893(3):398–408. [PubMed: 2888484]
32. Korshunov SS, Skulachev VP, Starkov AA. High protonic potential actuates a mechanism of production of reactive oxygen species in mitochondria. FEBS Lett 1997;416(1):15–8. [PubMed: 9369223]
33. Kushmerick M, Meyer R, Brown T. Regulation of oxygen consumption in fast-and slow twitch muscle. Am J Physiol 1992;263:(32):C598–C606. [PubMed: 1415510]
34. Kushmerick MJ. Energy balance in muscle activity: simulations of ATPase coupled to oxidative phosphorylation and to creatine kinase. Comp Biochem Physiol B Biochem Mol Biol 1998;120(1): 109–23. [PubMed: 9787781]
35. Kushmerick MJ, Moerland TS, Wiseman RW. Mammalian skeletal muscle fibers distinguished by contents of phosphocreatine, ATP, and Pi. Proc Natl Acad Sci U S A 1992;89(16):7521–5. [PubMed: 1502163]
36. Kuzmiak-Glancy S, Willis WT. Skeletal muscle fuel selection occurs at the mitochondrial level. J Exp Biol 2014;217(Pt 11):1993–2003. [PubMed: 24625643]
37. Kuzmiak S, Glancy B, Sweazea KL, Willis WT. Mitochondrial function in sparrow pectoralis muscle. J Exp Biol 2012;215(Pt 12):2039–50. [PubMed: 22623192]
38. Lefort N, Glancy B, Bowen B, et al. Increased reactive oxygen species production and lower abundance of complex I subunits and carnitine palmitoyltransferase 1B protein despite normal mitochondrial respiration in insulin-resistant human skeletal muscle. Diabetes 2010;59(10):2444–52. [PubMed: 20682693]
39. Lemasters JJ, Billica WH. Non-equilibrium thermodynamics of oxidative phosphorylation by inverted inner membrane vesicles of rat liver mitochondria. J Biol Chem 1981;256(24):12949–57. [PubMed: 7309743]
40. Maguire JJ, Davies KJ, Dallman PR, Packer L. Effects of dietary iron deficiency of iron-sulfur proteins and bioenergetic functions of skeletal muscle mitochondria. Biochimica et biophysica acta 1982;679(2):210–20. [PubMed: 7059584]
41. Masuda T, Dobson GP, Veech RL. The Gibbs-Donnan near-equilibrium system of heart. J Biol Chem 1990;265(33):20321–34. [PubMed: 2147022]
42. Messer JI, Jackman MR, Willis WT. Pyruvate and citric acid cycle carbon requirements in isolated skeletal muscle mitochondria. Am J Physiol Cell Physiol 2004;286(3):C565–72. [PubMed: 14602577]
43. Meyer R, Foley J. Testing models of respiratory control in skeletal muscle. Med Sci Sports Exerc 1994;26:52–7. [PubMed: 8133739]
44. Meyer RA. A linear model of muscle respiration explains monoexponential phosphocreatine changes. Am J Physiol 1988;254(4 Pt 1):C548–53. [PubMed: 3354652]
45. Meyer RA, Sweeney HL, Kushmerick MJ. A simple analysis of the “phosphocreatine shuttle”. Am J Physiol 1984;246(5 Pt 1):C365–77. [PubMed: 6372517]
46. Mitchell P, Moyle J. Evidence discriminating between the chemical and the chemiosmotic mechanisms of electron transport phosphorylation. Nature 1965;208(16):1205–6. [PubMed: 5870319]
47. Mracek T, Pecinova A, Vrbacky M, Drahota Z, Houstek J. High efficiency of ROS production by glycerophosphate dehydrogenase in mammalian mitochondria. Archives of biochemistry and biophysics 2009;481(1):30–6. [PubMed: 18952046]
48. Murphy MP, Brown GC, Brand MD. Thermodynamic limits to the stoichiometry of H+ pumping by mitochondrial cytochrome oxidase. FEBS Lett 1985;187(1):16–20. [PubMed: 2991005]
49. Nicholls D, Ferguson S. Bioenergetics 3 Amsterdam: Academic; 2002 288 p.
50. Nicholls DG, Bernson VS. Inter-relationships between proton electrochemical gradient, adenine-nucleotide phosphorylation potential and respiration, during substrate-level and oxidative phosphorylation by mitochondria from brown adipose tissue of cold-adapted guinea-pigs. Eur J Biochem 1977;75(2):601–12. [PubMed: 18347]

51. Ohira Y, Cartier LJ, Chen M, Holloszy JO. Induction of an increase in mitochondrial matrix enzymes in muscle of iron-deficient rats. Am J Physiol 1987;253(5 Pt 1):C639–44. [PubMed: 3479908]
52. Onishi T, Kroger A, Heldt HW, Pfaff E, Klingenberg M. The response of the respiratory chain and adenine nucleotide system to oxidative phosphorylation in yeast mitochondria. Eur J Biochem 1967;1(3):301–11. [PubMed: 4293926]
53. Onsager L Reciprocal relations in irreversible processes. I. Phys Rev 1931;37(4):405–26.
54. Onsager L Reciprocal relations in irreversible processes. II. Phys Rev 1931;38(12):2265–79.
55. Pate E, Cooke R. Addition of phosphate to active muscle fibers probes actomyosin states within the powerstroke. Pflugers Arch 1989;414(1):73–81. [PubMed: 2726438]
56. Pate E, Franks-Skiba K, Cooke R. Depletion of phosphate in active muscle fibers probes actomyosin states within the powerstroke. Biophys J 1998;74(1):369–80. [PubMed: 9449337]
57. Rottenberg H The thermodynamic description of enzyme-catalyzed reactions. The linear relation between the reaction rate and the affinity. Biophys J 1973;13(6):503–11. [PubMed: 4714445]
58. Sahlin K, Katz A, Broberg S. Tricarboxylic acid cycle intermediates in human muscle during prolonged exercise. Am J Physiol 1990;259(5 Pt 1):C834–41. [PubMed: 2240197]
59. Schwerzmann K, Hoppeler H, Kayar SR, Weibel ER. Oxidative capacity of muscle and mitochondria: correlation of physiological, biochemical, and morphometric characteristics. Proc Natl Acad Sci U S A 1989;86(5):1583–7. [PubMed: 2922400]
60. Skulachev VP. Role of uncoupled and non-coupled oxidations in maintenance of safely low levels of oxygen and its one-electron reductants. Q Rev Biophys 1996;29(2):169–202. [PubMed: 8870073]
61. Starkov AA, Fiskum G. Regulation of brain mitochondrial H2O2 production by membrane potential and NAD(P)H redox state. J Neurochem 2003;86(5):1101–7. [PubMed: 12911618]
62. Stucki JW. The optimal efficiency and the economic degrees of coupling of oxidative phosphorylation. Eur J Biochem 1980;109(1):269–83. [PubMed: 7408881]
63. Sweeney H The importance of the creatine kinase reaction: the concept of metabolic capacitance. Med Sci Sports Exerc 1994;26:30–6. [PubMed: 8133735]
64. Terjung RL, Baldwin KM, Winder WW, Holloszy JO. Glycogen repletion in different types of muscle and in liver after exhausting exercise. Am J Physiol 1974;226(6):1387–91. [PubMed: 4833994]
65. Utter AC, Kang J, Robertson RJ, et al. Effect of carbohydrate ingestion on ratings of perceived exertion during a marathon. Medicine and science in sports and exercise 2002;34(11):1779–84. [PubMed: 12439083]
66. Van der Meer R, Westeroff HV, Van Dam K. Linear relation between rate and thermodynamic force in enzyme-catalyzed reactions. Biochim Biophys Acta 1980;591(2):488–93. [PubMed: 7397133]
67. Wanders RJ, Groen AK, Meijer AJ, Tager JM. Determination of the free-energy difference of the adenine nucleotide translocator reaction in rat-liver mitochondria using intra-and extramitochondrial ATP-utilizing reactions. FEBS Lett 1981;132(2):201–6. [PubMed: 6271588]
68. Watt IN, Montgomery MG, Runswick MJ, Leslie AG, Walker JE. Bioenergetic cost of making an adenosine triphosphate molecule in animal mitochondria. Proc Natl Acad Sci U S A 2010;107(39): 16823–7. [PubMed: 20847295]
69. Westerhoff HV, Hellingwerf KJ, Arents JC, Scholte BJ, Van Dam K. Mosaic nonequilibrium thermodynamics describes biological energy transduction. Proc Natl Acad Sci U S A 1981;78(6): 3554–8. [PubMed: 6267598]
70. Whipp BJ, Wasserman K. Oxygen uptake kinetics for various intensities of constant-load work. J Appl Physiol 1972;33(3):351–6. [PubMed: 5056210]
71. Willis WT, Dallman PR. Impaired control of respiration in iron-deficient muscle mitochondria. Am J Physiol 1989;257(6 Pt 1):C1080–5. [PubMed: 2610248]
72. Wilson D Factors affecting the rate and energetics of mitochondrial oxidative phosphorylation. Med Sci Sports Exerc 1994;26:37–43. [PubMed: 8133736]

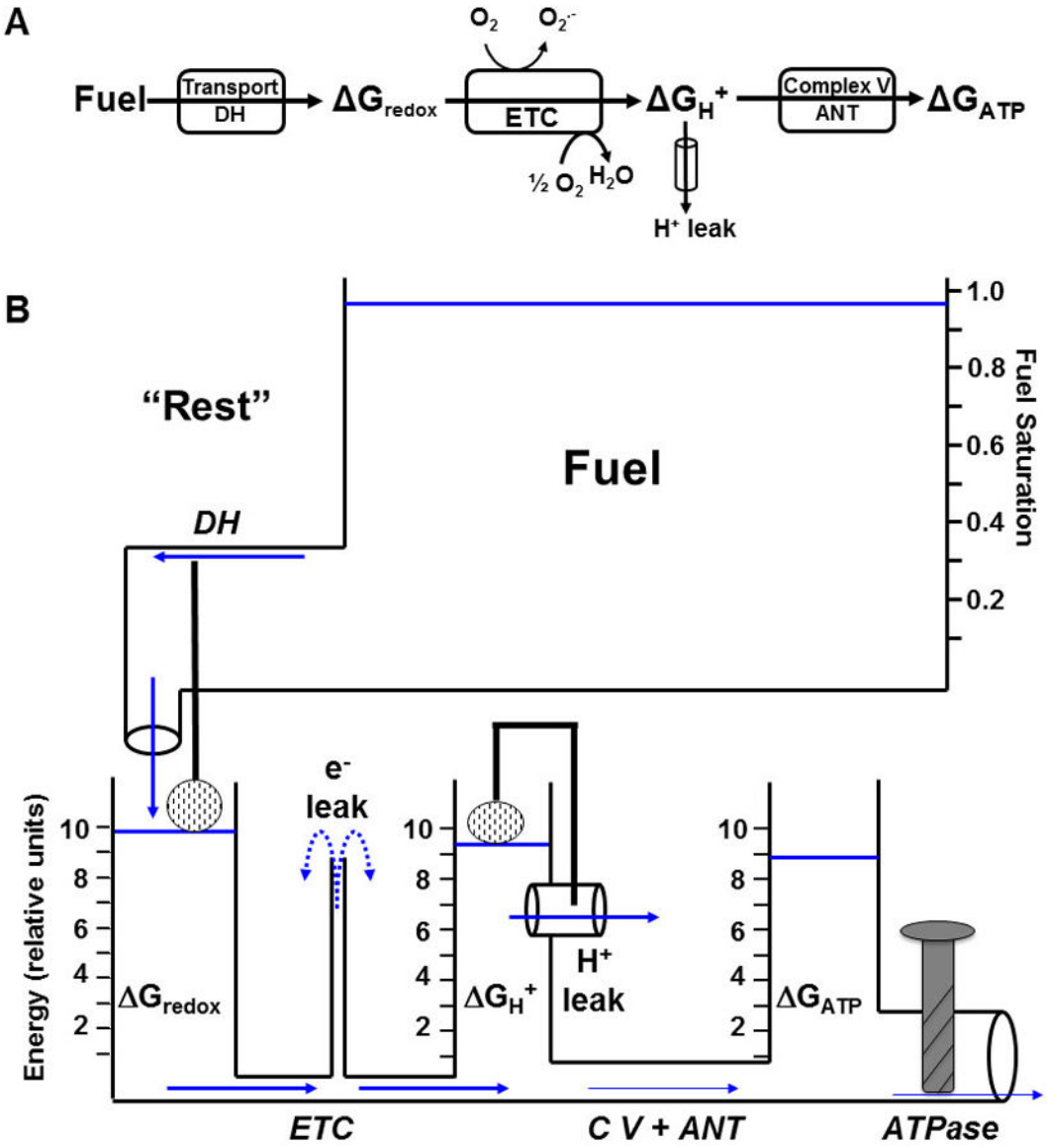

Figure 1: Simple Models of Oxidative Phosphorylation.

Modular (A) and hydraulic analog (B) models of oxidative phosphorylation showing the transduction of energy from oxidative fuels which are transported into the mitochondria and converted into matrix redox potential (ΔG_{redox}) by dehydrogenase enzymes (DH). ΔG_{redox} is then converted into a protonmotive force (Δp or ΔG_{H+}) by the electron transport chain (ETC). Δp is converted to ATP by Complex V (C V) and transported out of the mitochondria by adenine nucleotide translocase (ANT) where it contributes to the free energy of ATP hydrolysis (ΔG_{ATP}) available to be used by cytosolic ATPases. Electron leak ($O_2^{\cdot -}$) from the ETC and proton leak back across the inner mitochondrial membrane are also depicted. In the hydraulic model, the water level in each tank represents the availability of the respective free energy forms and the diameter of the pipes is proportional to the activity of the enzymes along that portion of the pathway. The height of the water in each tank exerts a pressure on both the upstream and downstream adjacent pipes. Water flow (or flux, J)

between two tanks is thus proportional to the difference in water levels between each tank ($\Delta G_1 - \Delta G_2$) as well as the size of the pipe (conductance, L) between them.

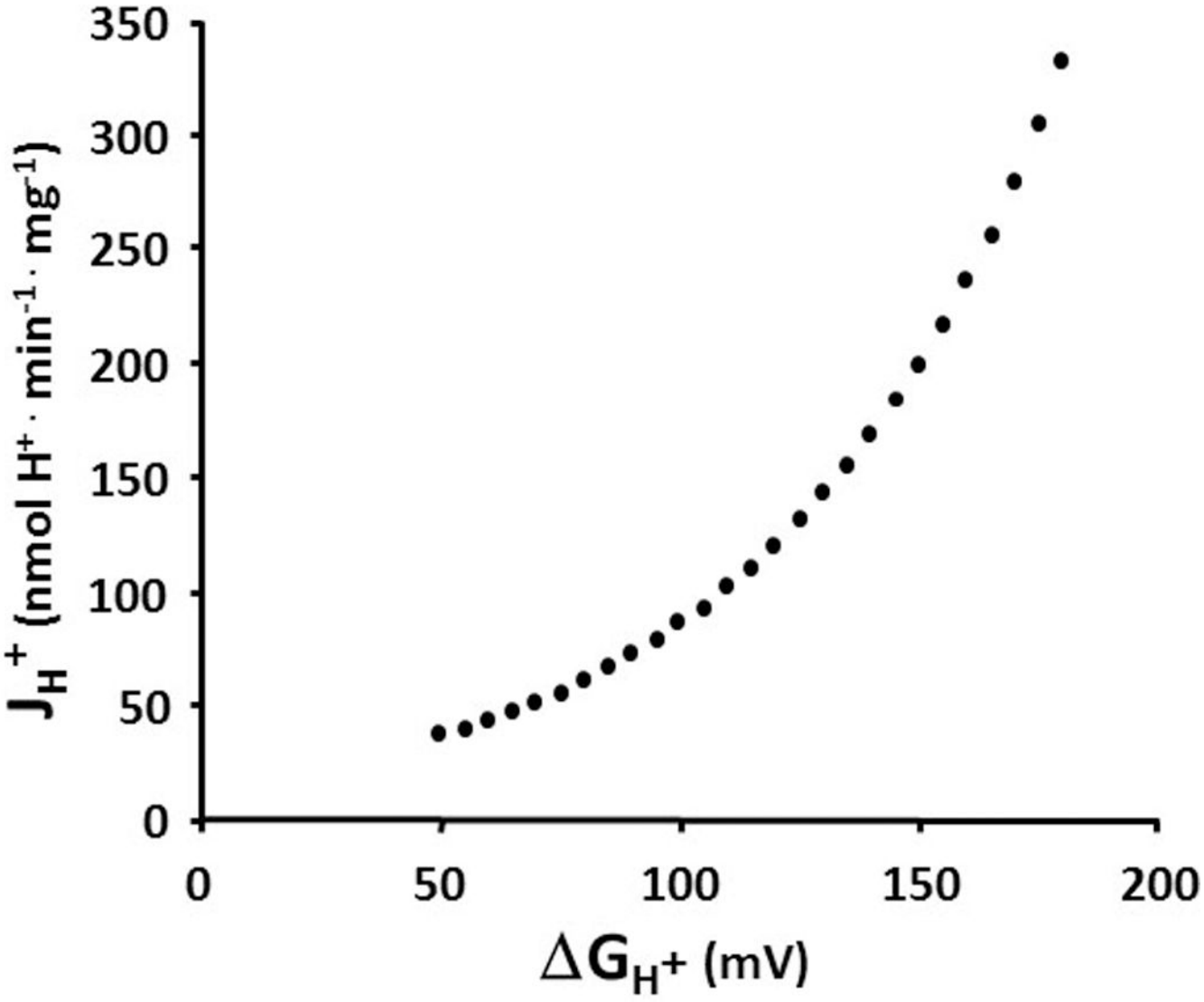

Figure 2: Mitochondrial Proton Leak Kinetics.

Non-phosphorylating proton flux back across the mitochondrial inner membrane in rat liver mitochondria increases exponentially with the proton motive force (ΔG_{H+}).

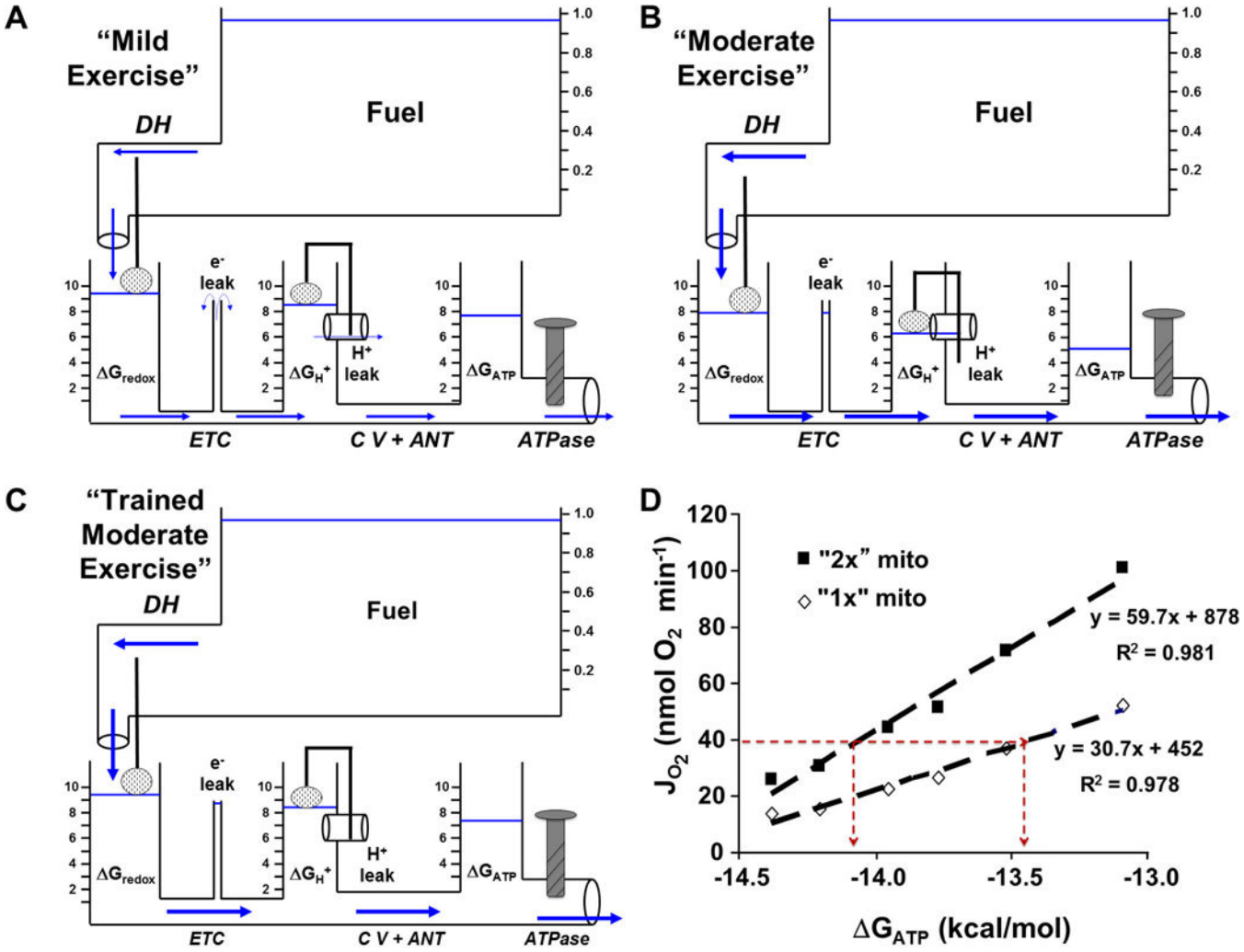

Figure 3: Effects of Exercise and Training.

A) Mild exercise in the hydraulic model. A mild increase in cellular contractile activity slightly opens the ATPase valve and water flow through the ATPase pipe (ATP utilization) causes the ΔG_{ATP} tank water level to fall. In turn, water flow (fuel oxidation and ATP synthesis) from upstream tanks increases to match the demand (steady state ATP turnover). B) Simulating moderate exercise by a larger opening of the ATPase valve (more contractile activity) results in even greater water flow (ATP sythesis) and a further fall in the level of the water tanks (free energies). Note that with the lower levels of the water tanks, the leak reactions are reduced. C) Endurance training resulting in increased mitochondrial content in skeletal muscle is depicted as an increase in pipe diameters. Repeating the "moderate exercise" bout by opening the ATPase valve (same contractile activity) to the same level as in B now results in better maintenance of the water levels in the tanks (free energies). D) Experimental support for the hydraulic model predictions in C. Doubling mitochondrial content results in a greater free energy level (ΔG_{ATP}) at a given rate of oxygen consumption (J_{O2}) in isolated rat hindlimb skeletal muscle mitochondria.

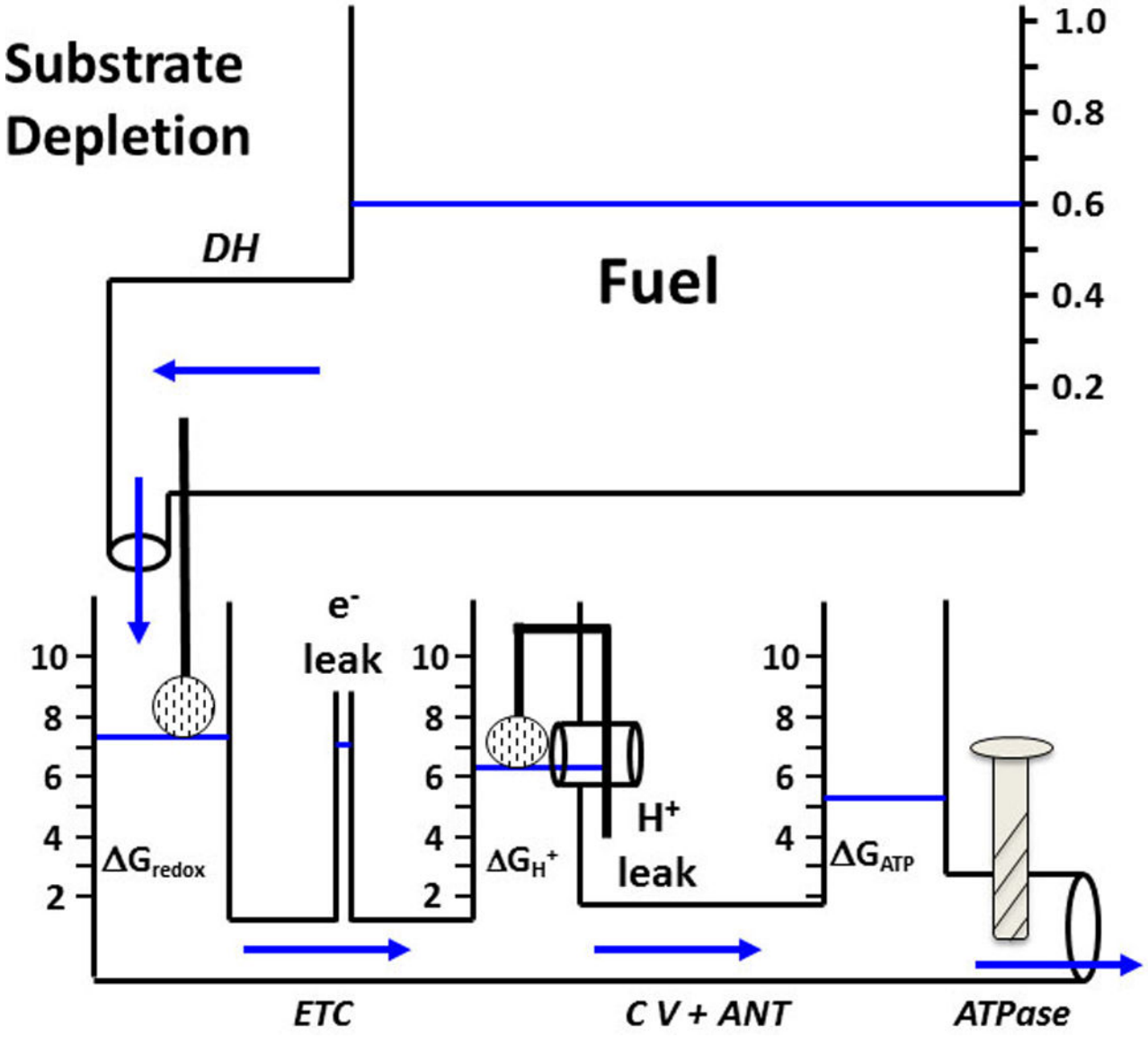

Figure 4: Effect of Reduced Fuel Availability.

Substrate depletion simulated by reducing the water level in the fuel tank results in lower water levels (free energies) in the downstream tanks and drives less water flow (lower ATP production). Compare with Figure 3C.

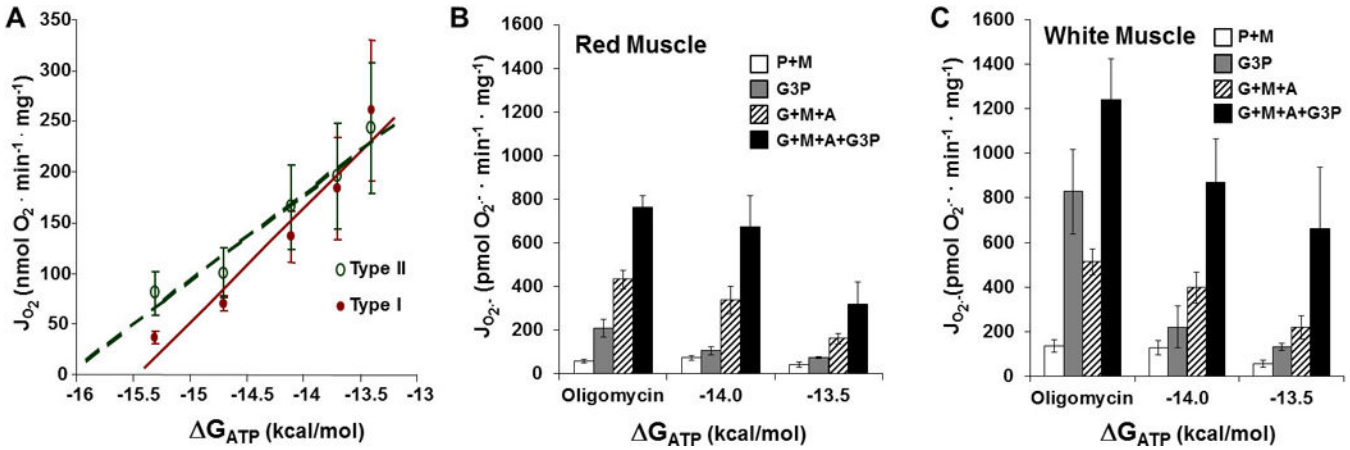

Figure 5: Differences between Fast and Slow Twitch Muscle Mitochondria.

A) Mitochondria isolated from rabbit gracilis (Type II, glycolytic) muscle maintain a higher free energy level (ΔG_{ATP}) at a given oxygen consumption rate (J_{O2}) than soleus (Type I, oxidative) muscle mitochondria. Greater free energy availability (higher water levels) in the hydraulic model predicts increases in the leak reactions. Mitochondria isolated from rat white, glycolytic hindlimb muscle produce more superoxide (C) than mitochondria isolated from red, oxidative hindlimb muscle (B) under conditions simulating rest (oligomycin) and mild (−14.0) and moderate (−13.5) exercise. P+M: pyruvate (1 mM) and malate (1 mM), G3P: glycerol 3-phosphate (10 mM), G+M+A: glutamate (10 mM), malate (1 mM), and arsenite (10 mM).

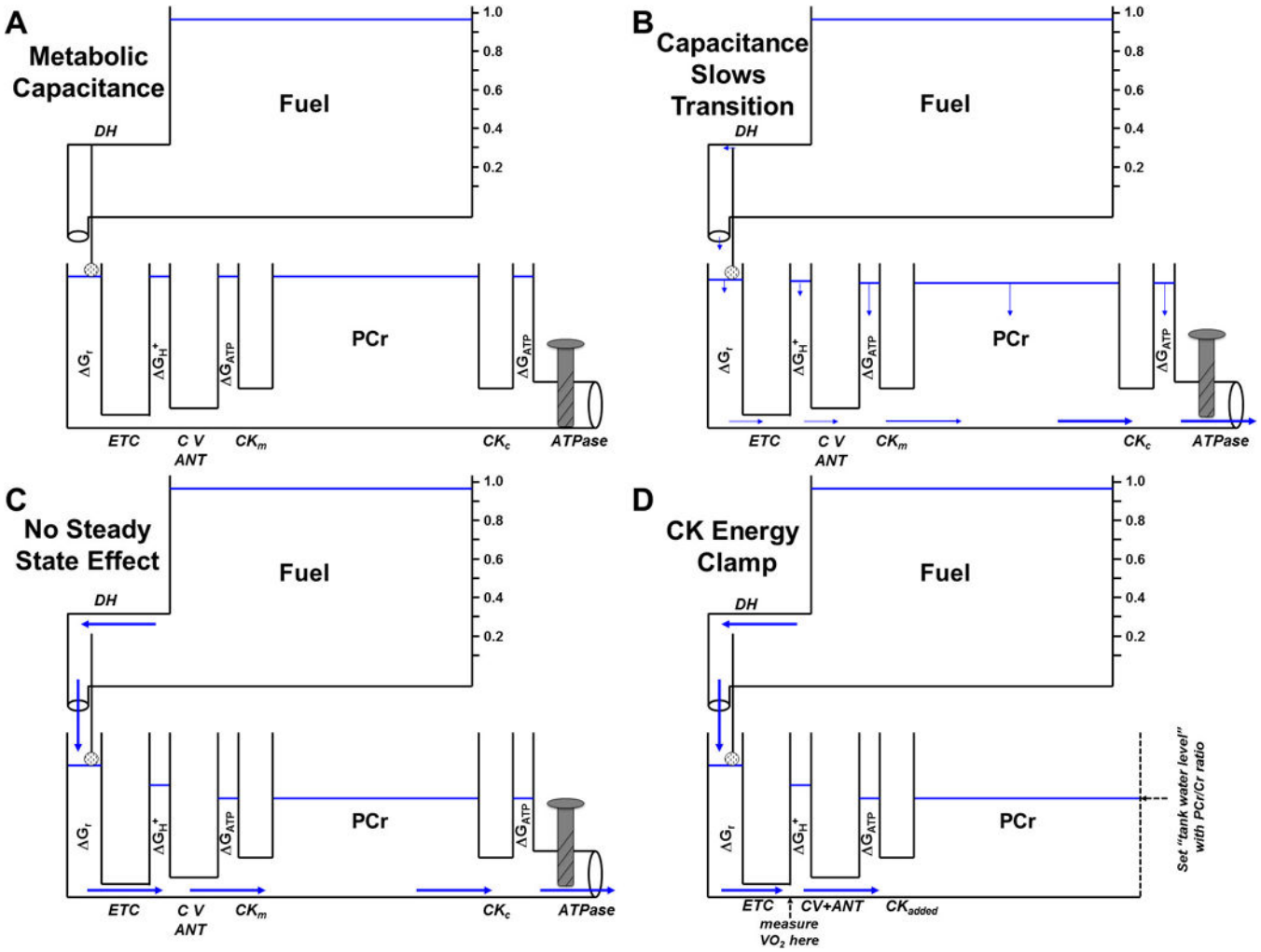

Figure 6: Capacitance of the Creatine Pool.

A) Addition of a high capacitance water tank with adjacent large diameter pipes to the hydraulic model representing the high concentrations of phosphocreatine (PCr) and creatine kinase (CK) and equilibrium with ΔG_{ATP} in skeletal muscle. B) Upon opening the ATPase valve, the transition to steady state is slowed due to the large amount of water in the PCr tank. C) The large PCr capacitance does not affect steady state height of the other water tanks. D) The Creatine Kinase Energy Clamp. In isolated mitochondria with no added ATPase, ΔG_{ATP} can be set and maintained at steady state by adding saturating CK, 5 mM ATP, and known ratios of PCr and creatine (Cr). In the presence of a constant fuel source, the resulting water flow (metabolic flux) is thus completely controlled by the diameters of the pipes (effective mitochondrial enzyme activities).

Table 1:
Contribution of Each Pathway to the Total Mitochondrial Resistance to Energy Transfer.

The calculated resistances of 1) fuel transport and dehydrogenase activity (DH), 2) ETC activity (ETC), and 3) ATP synthase and ANT (CV + ANT) to the total resistance of the energy transduction pathway in the absence and presence of Ca^{2+}.

Mitochondrial Resistance to Energy Transfer (Ohms)				
Segment	**No Calcium**		**+ Calcium (840 nM)**	
	Resistance	% Total	Resistance	% Total
Dehydrogenases	25.6	9.1	15.1	12.6
Electron Transport Chain	171.5	60.8	70.2	58.3
Complex V + ANT	84.8	30.1	35.0	29.1
Total	281.9	100.0	120.4	100.0